# Distributed Actin Turnover in the Lamellipodium and FRAP Kinetics

Matthew B. Smith[1], Tai Kiuchi[2], Naoki Watanabe[2], Dimitrios Vavylonis[1]

[1] Department of Physics, Lehigh University, Bethlehem PA 18015

[2] Laboratory of Single-Molecule Cell Biology, Tohoku University Graduate School of Life Sciences, Sendai, Miyagi 980-8578, Japan

# Supplementary Material

### 1. Calculation of the steady state F-actin profile based on single molecule speckle statistics

To obtain an analytical expression for the F-actin profile based on SiMS data, we substitute Eqs. (1) and (2) into (4) and (3) of the main text to obtain

$$F(x) = \frac{G_\infty K}{v_r} \sum_{i=1}^{2} \sum_{j=1}^{2} F_{ij}(x) , \tag{S1}$$

where:

$$F_{ij}(x) = \frac{A_i C_j \tau_j}{1/(v_r \tau_j) - 1/\lambda_i} \left( e^{-x/\lambda_i} - e^{-x/(v_r \tau_j)} \right) \quad \text{if} \quad v_r \tau_j \neq \lambda_i \tag{S2}$$

or

$$F_{ij}(x) = A_i C_j \tau_j \, e^{-x/(v_r \tau_j)} x \quad \text{if} \quad v_r \tau_j = \lambda_i \tag{S3}$$

For both cases when we solve for the total amount of F-actin, we get the same result,

$$\int_0^\infty F(x) dx = G_\infty K \sum_{i=1}^{2} \sum_{j=1}^{2} A_i C_j \tau_j^{\,2} \lambda_i \, . \tag{S4}$$

This result demonstrates that the F-actin concentration is directly proportional to parameter *K*.

### 2. Condition on model parameters to generate positive G-actin profile.

The G-actin profile can be calculated analytically by substituting Eq. (S4) into Eq. (6) of the main text. From Eq. (S4) we calculate that G-actin at the leading edge will go to zero when

$$\frac{G(0)}{G_\infty} = 1 - \frac{v_r}{D} K \sum_{i=1}^{2} \sum_{j=1}^{2} A_i C_j \tau_j{}^2 \lambda_i \qquad \text{(S5)}$$

This yields the following inequality that should be satisfied such that $G(0)$ does not become negative:

$$D > v_r K \sum_{i=1}^{2} \sum_{j=1}^{2} A_i C_j \tau_j{}^2 \lambda_i \,. \qquad \text{(S6)}$$

**3. Picking speckle lifetimes and initializing steady state in stochastic simulations**

When a G-actin or O-actin subunit associates to become F-actin, its lifetime as F-actin is picked from the double exponential lifetime distribution of Eq. (2), a sum of "long-life" and "short-life" exponentials. We first pick one of the exponentials with probabilities.

$$p(2) = \frac{\tau_2 C_2}{\tau_2 C_2 + \tau_1 C_1}, \quad p(1) = 1 - p(2). \qquad \text{(S7)}$$

Then we pick the actual lifetime from the respective exponential distribution.

To initialize the simulations, we distribute particles in space according to the analytically-calculated F-, O- and G-actin distributions. When choosing the lifetime of a particle at distance $x$ from the leading edge in the initial state, we must be careful to recognize the possible paths this subunit could have taken to arrive at $x$. Consider a subunit that converts to F-actin at $x$' whose lifetime belongs to either the long- or short-lived population ($i$ = 1 or 2). The probability that the subunit will still exist at $x$ is based on the time it needs to get there:

$$p(x \mid i, x') = e^{-\frac{x - x'}{v_r \tau_i}} \qquad \text{(S8)}$$

Knowing the distribution of appearances, $a(x)$, we can calculate the probability of finding a subunit of type $i$ at $x$:

$$p(x \mid i) = \Lambda \int_0^x a(x') e^{-\frac{x - x'}{v_r \tau_i}} dx, \qquad \text{(S9)}$$

where $\Lambda$ is a normalization constant that does not depend on $i$. Thus we can apply Bayes' theorem to determine the probability that a subunit found at $x$ belongs to the long-life population:

$$p(2 \mid x) = \frac{p(x \mid 2) p(2)}{p(x \mid 2) p(2) + p(x \mid 1) p(1)}, \qquad \text{(S10)}$$

and similarly for $p(1|x)$. During initialization, when a subunit is placed at $x$, the above probability was used to determine if the lifetime of the subunit is picked from the long-life exponential distribution or the

short-life distribution. This expression also gives a way to calculate an effective time constant as a function of position.

$$\tau_{eff}(x) = \tau_2 p(2 \mid x) + \tau_1 p(1 \mid x). \quad \text{(S11)}$$

The O-actin lifetimes were picked from a single exponential distribution with average lifetime $\tau_{O.}$

We tested that the simulations maintain the initial steady state over time, thus validating our procedure. Fig. S2A shows that the values of local concentrations do not change significantly, and Fig S2B shows that the shape of the concentration profile is the same over time.

**4. FRAP measurements of F-actin turnover in XTC cells**

To measure F-actin turnover in lamellipodia precisely using FRAP, we performed dual-color FRAP, also called FLAP (fluorescence localization after photobleaching), where the fluorescence recovery of one fluorescent species after its photobleaching is measured relative to the other fluorescent species as in reference (1). This method normalizes the data for the fluctuation of the system and enables accurate follow-up of FRAP labels over very long times owing to the ratiometric measurement. XTC cells were transfected with two expression vectors encoding EGFP- and mCherry-tagged actin. The fluorescence recovery of EGFP-actin after its photobleaching showed the rate of F-actin turnover. The fluorescence of mCherry-actin was used to monitor the changes in the local actin content. The time-lapse imaging of EGFP- and mCherry-actin were performed at 3 sec intervals using an Olympus X71 microscope equipped with Olympus PlanApo NA1.40 100X objective lens and an EM-CCD camera (Evolve 512, Photometrics) controlled by MetaMorph software (Molecular Device). After the 10th image acquisition, EGFP-actin was photobleached with ten times 435 nm laser pulses within 300 ms using the MicroPoint laser system (Photonic Instruments), and image acquisition was immediately restarted.

To quantify FRAP recovery at the leading edge, we tracked the leading edge position in the unbleached mCherry-actin channel with active contours (2,3). We chose cells that had retrograde flow ~55nm/s (measured using the bleached channel) and a leading edge that moves less than 0.6 μm during recovery. The region of the image to the right side of the contour is outside the cell and was used to calculate the out-of-cell backgrounds $B_C$ and $B_E$ of the mCherry and EGFP channels. The image ratio $r(x,y,t)$ at position $x,y$ and time $t$ was calculated using:

$$r(x,y,t) = \frac{E(x,y,t) - B_E(t)}{C(x,y,t) - B_C(t)}, \quad \text{(S12)}$$

where $E(x,y,t)$ and $C(x,y,t)$ are the EGFP and mCherry-actin intensities at $x,y$ and time $t$. The normalized fluorescence recovery $< r_{a-b}(t) >^*$ in a region between distances $a$ and $b$ from the leading edge was calculated using:

$$< r_{a-b}(t) >^* = \frac{< r_{a-b}(t) > - < r^{prebleach} >}{< r^{prebleach} > - < r(0) >}. \quad \text{(S13)}$$

Here $< r_{a-b}(t) >$ is the average value of the image ratio between *a* and *b*, $< r^{prebleach} >$ is the average value of the image ratio at the lamellipodium for 10 frames prior to bleach (30 s), and $< r(0) >$ is the value of the image ratio in the first frame after the bleach.

**5. Calculating the error between simulation and experiment.**

The error is calculated by using the sum of squared error between the simulation and the averaged recovery curves of Fig. 2C. For every experimental data point after photobleaching, the difference between the corresponding fractional recovery in simulations is squared. All of these values are summed together (for both front and back recovery curves) to get the final error.

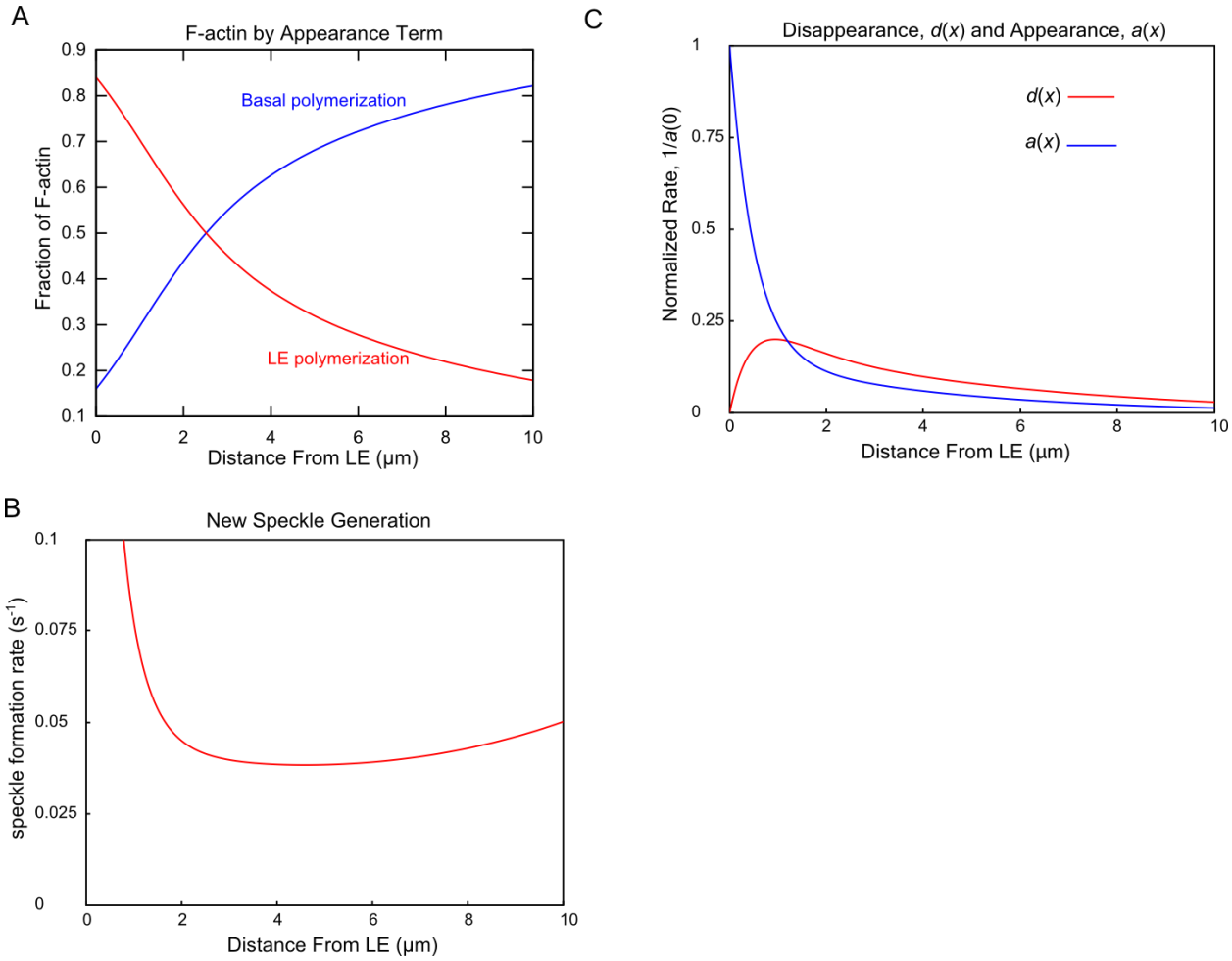


**Figure S1.** Calculations based on single molecule speckle statistics to compare with results in (4). The parameters are the same as in Fig. 3 and the curves are the same for both values of $K$. (A) Analytical results showing the amount of F-actin due to leading edge (LE) or the basal polymerization, using Eqs. (S1)-(S3). Here we define LE polymerization to be the polymerization events due to the first term in Eq. (1) (the term proportional to $A_1$). Basal polymerization corresponds to the second term (proportional to $A_2$). The resulting curves are similar to Fig. 4B of Ref. (4). (B) Plot of relative new speckle formation rate vs distance from LE. This is the rate of speckle appearance, $a(x)$, divided by the amount of F-actin at each location, $F(x)$, calculated using Eqs. (S1)-(S3). The graph is similar to the experimental measurements in Fig. 3B of Ref. (4) where the value of the new speckle formation rate was around 0.03 $s^{-1}$. (C) Disassembly rate (Eq. 5) as a function of distance from the leading edge normalized to the appearance rate, $a(x)$, at $x = 0$.

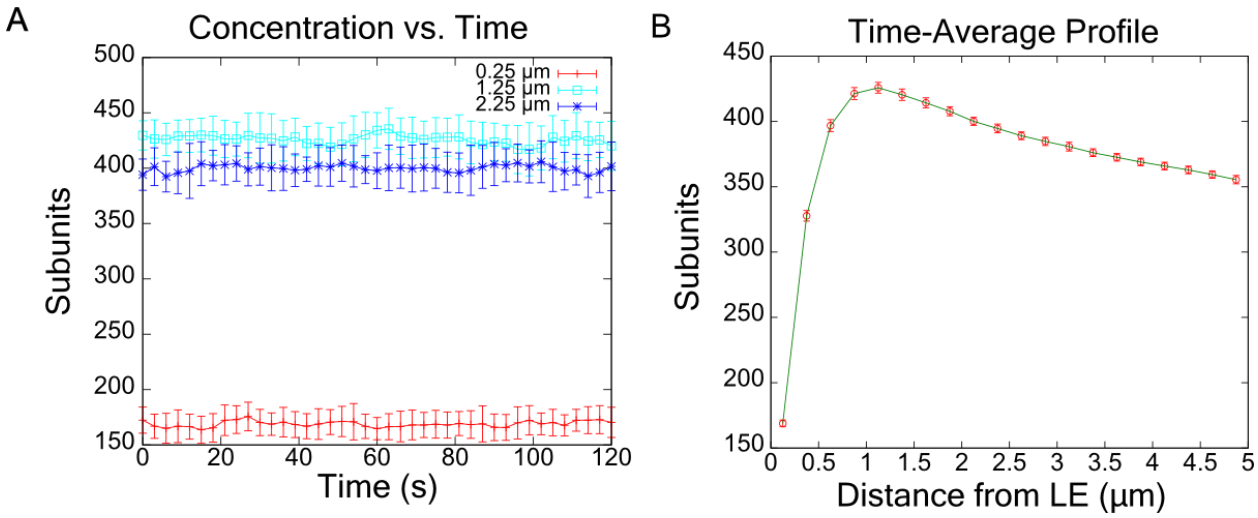


**Figure S2.** Stochastic particle simulation maintains steady state initialized according to analytical expressions for steady state profiles and Eq. (S10). Example showing monomer-only model with $K$ = 0.5 $s^{-1}$, $v_r$ = 0.03 µm/s. (A) 100 simulations with an area of 55 µm x 40 µm were started with the system in steady state. Each system was divided into strips of width 0.25 µm and the number of particles in the strip was measured every 3 s. The values plotted are the average measured value for strips at three different positions. Error bars are the standard deviation among simulations. (B) All of the 0.25 µm strips from 0 to 5 µm were averaged over time from 0 to 120 s to create a profile. The size of the error bars are the standard deviation of the average value sampled every 3 s for 120 s.

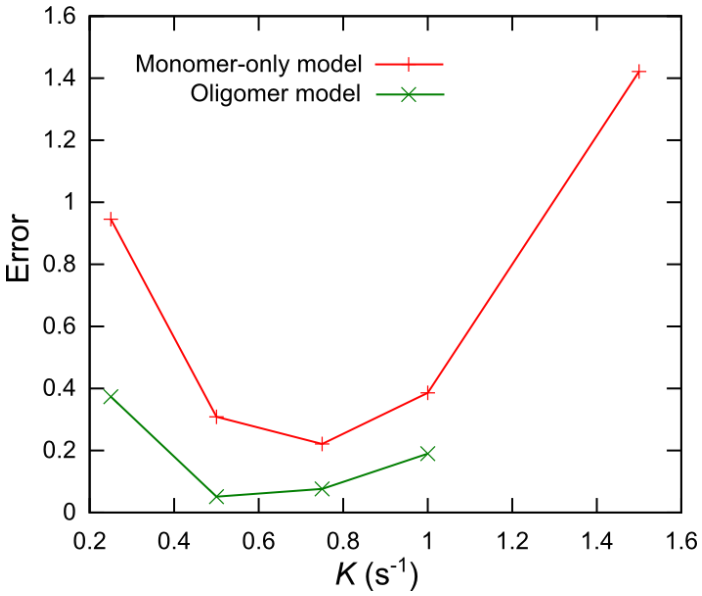


**Figure S3.** The effects of changing parameter *K* (influencing the F:G ratio) on the error between simulated and experimental FRAP curves. Monomer-only model uses same parameters as in Fig. 4. The model with oligomers uses same parameters as in Fig. 6. The oligomer model gives better fits to the data for values of *K* between 0.5-0.8 $s^{-1}$that reproduce F:G ratios consistent with prior experiments, see Fig. 5. The figure does not include large values of *K* that would give negative concentrations, see Eq. (S6).

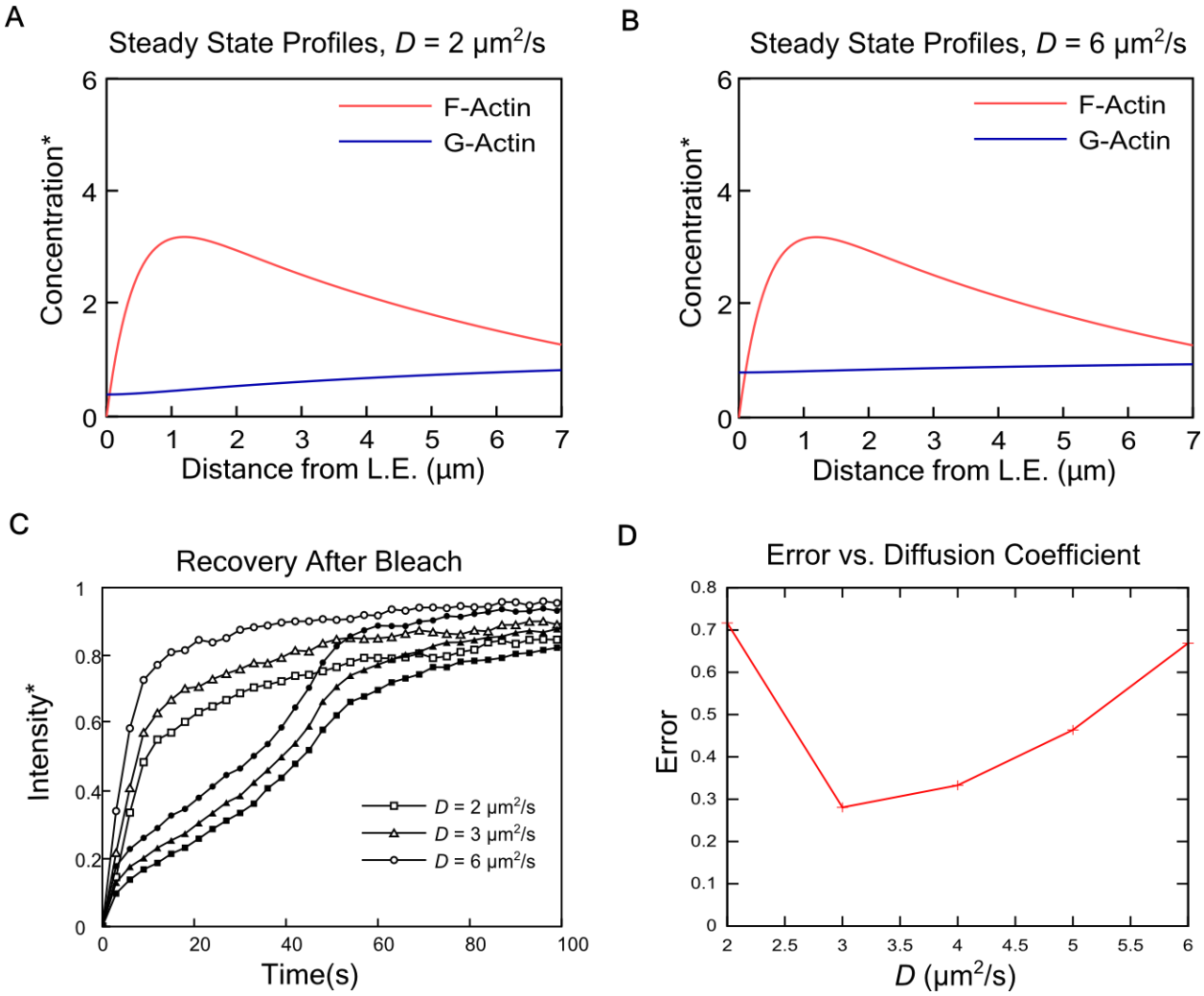


**Figure S4.** Effects on profile and FRAP due to changing the diffusion coefficient in monomer-only model. The other parameters remain the same, $K = 0.5\ s^{-1}$ and $v_r = 0.056$ μm/s. Steady state profiles for (A) $D = 2\ \mu m^2/s$, and (B) $D = 6\ \mu m^2/s$. (C) Comparison of FRAP recovery results for different values of $D$ (front: empty symbols; back: filled symbols). (D) Sum of error for FRAP simulations compared to the experimental data of Fig. 2C. Decreasing $D$ increases the gradient of the G-actin profile and slows down FRAP recovery at both the front and the back of the lamellipodium. Some studies have suggested $D$ values as large as 14 $\mu m^2/s$ (5). For such large values of $D$ the G-actin profile becomes flat and the FRAP curves approach remain similar to those of $D = 6\ \mu m^2/s$.

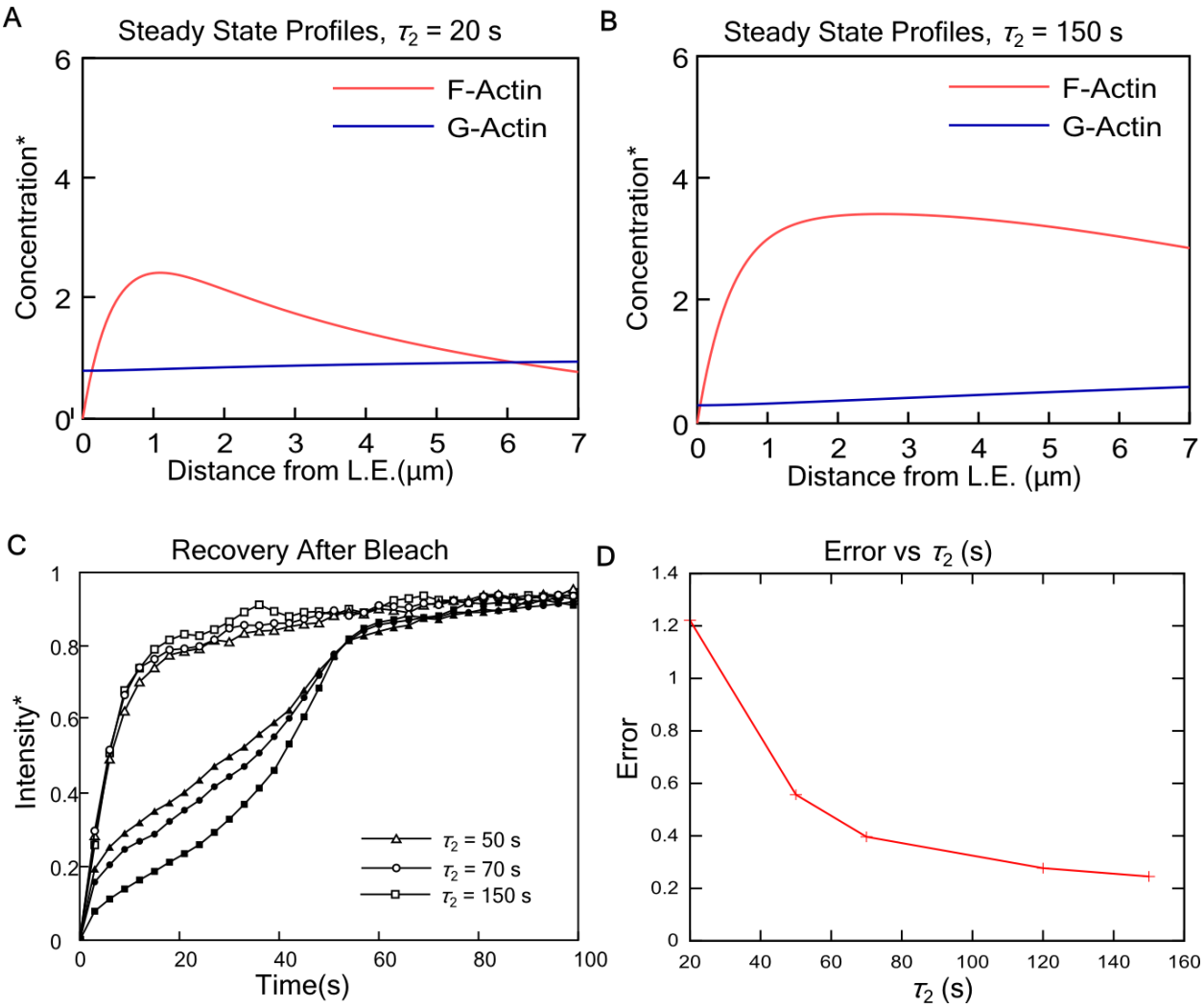


**Figure S5.** Effects on concentration profile and FRAP in monomer-only model due to changing value of parameter $\tau_2$ that describes the lifetime of the "long-lived" F-actin subunits, see Eq. (2). We use $K$= 0.5 $s^{-1}$ and $v_r$ = 0.056 μm/s. The value of $\tau_2$ used in the main text was 60 s. Steady state profiles for (A) $\tau_2$ = 20 s and (B) $\tau_2$ = 150 s. (C) Comparison of FRAP recovery results for different values of $\tau_2$ (front: empty symbols; back: filled symbols). (D) Error for FRAP simulations compared to the experimental data of Fig. 2C. The error decreases with increasing $\tau_2$ but the lamellipodium becomes very extended as shown in panel B.

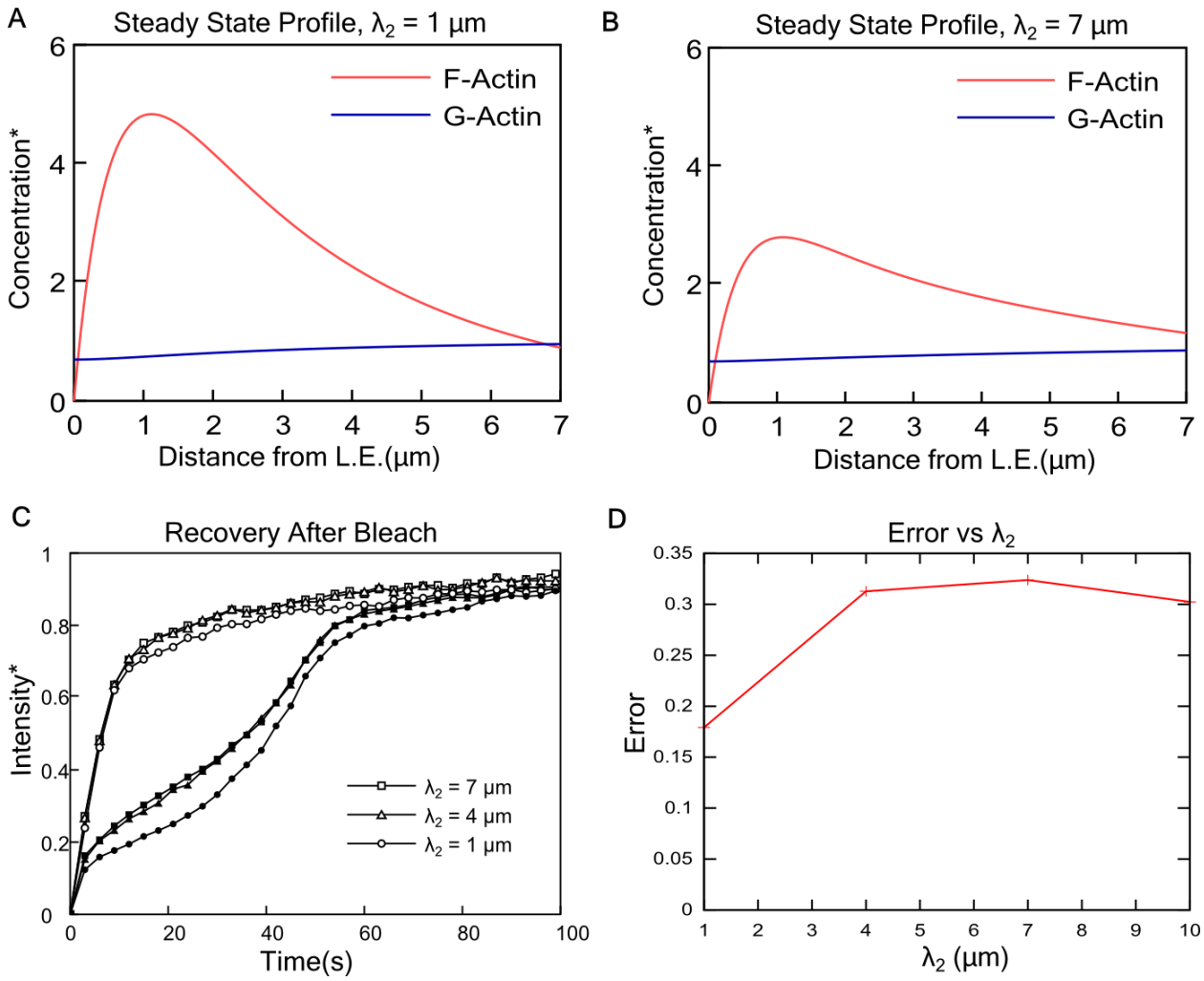


**Figure S6**. Effects on concentration profile and FRAP in monomer-only model due to changing value of parameter $\lambda_2$ in Eq. (1), which determines how far into the lamellipodium polymerization occurs. The value of $\lambda_2$ used in the main text was 4 μm. The total appearances rate corresponding to each exponential term of Eq. (1) was fixed by keeping $KA_2\lambda_2$ and $KA_1\lambda_1$ constant. All other parameters were kept the same as in Fig. 4: $\lambda_1$ = 0.5 μm, $v_r$ = 0.056 μm/s. (A) $\lambda_2$ = 1 μm, $K$ = 0.74 $s^{-1}$, $A_1$ = 0.57, $A_2$ = 0.43. (B) $\lambda_2$ = 7 μm, $K$ = 0.46 $s^{-1}$, $A_1$ = 0.9, $A_2$ = 0.1. (C) Recovery plot comparing three different recovery curves for the different $\lambda_2$ (front: empty symbols; back: filled symbols). (D) Error for FRAP simulations compared to the experimental data of Fig. 2C.

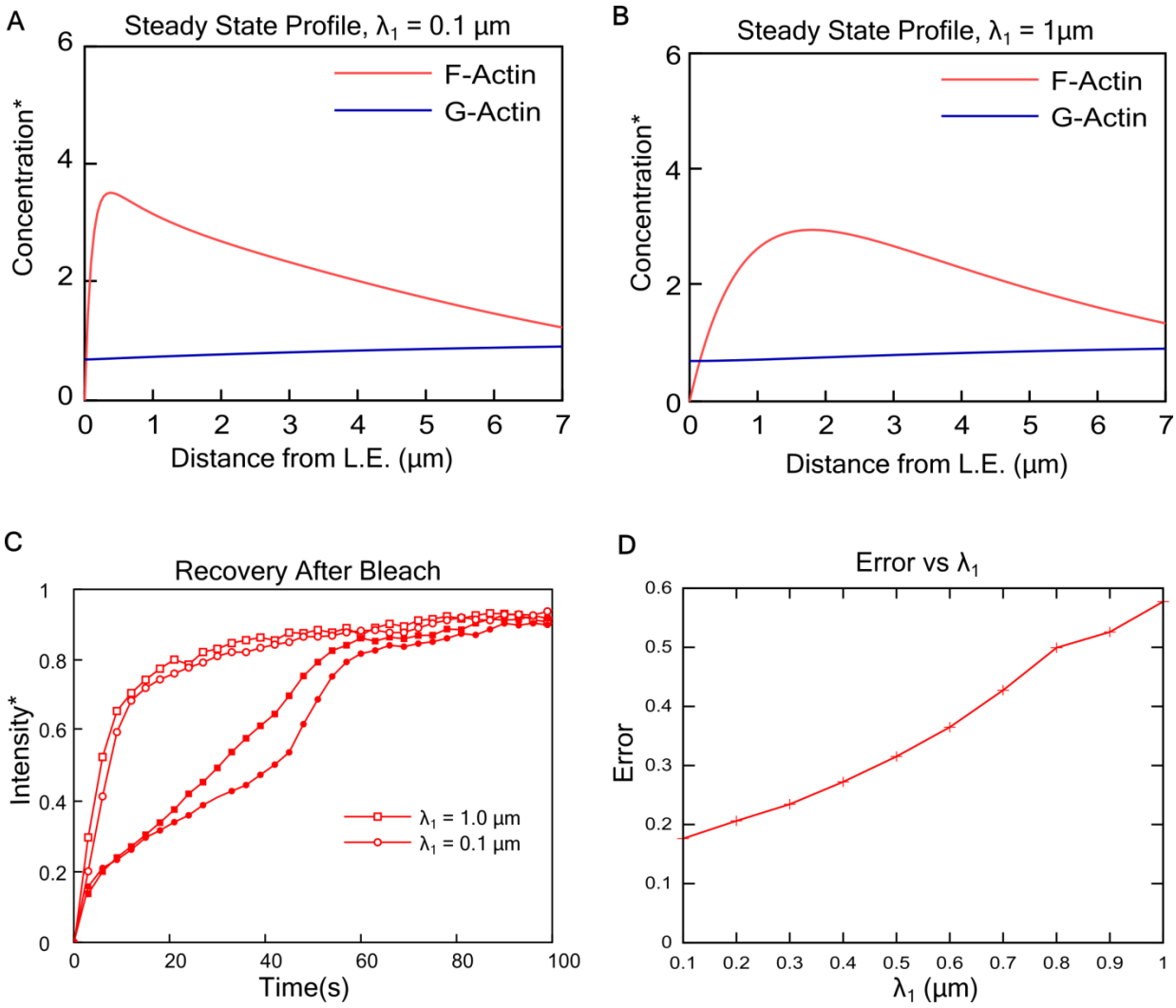


**Figure S7.** Effects on concentration profile and FRAP due to changing value of parameter $\lambda_1$ in Eq. (1), which determines the width of the polymerization region near the leading edge. The value of $\lambda_1$ used in the main text was 0.5 μm. The total appearance rate corresponding to each exponential term of Eq. (1) was fixed by keeping $KA_2\lambda_2$ and $KA_1\lambda_1$ constant. (A) $\lambda_1$ = 0.1 μm, $K$ = 2.18 $s^{-1}$, $A_1$ = 0.96, $A_2$ = 0.04, and (B) $\lambda_1$ =1.0 μm, $K$ = 0.29 $s^{-1}$, $A_1$ = 0.72, $A_2$ = 0.28. Panels A and B show results of the monomer-only model with all other parameters kept the same as in Fig. 4: $\lambda_2$ = 4 μm, $v_r$ = 0.056 μm/s. (C) Recovery curves for different values of $\lambda_1$. (D) Error for FRAP simulations compared to the experimental data of Fig. 2C, as function of $\lambda_1$.

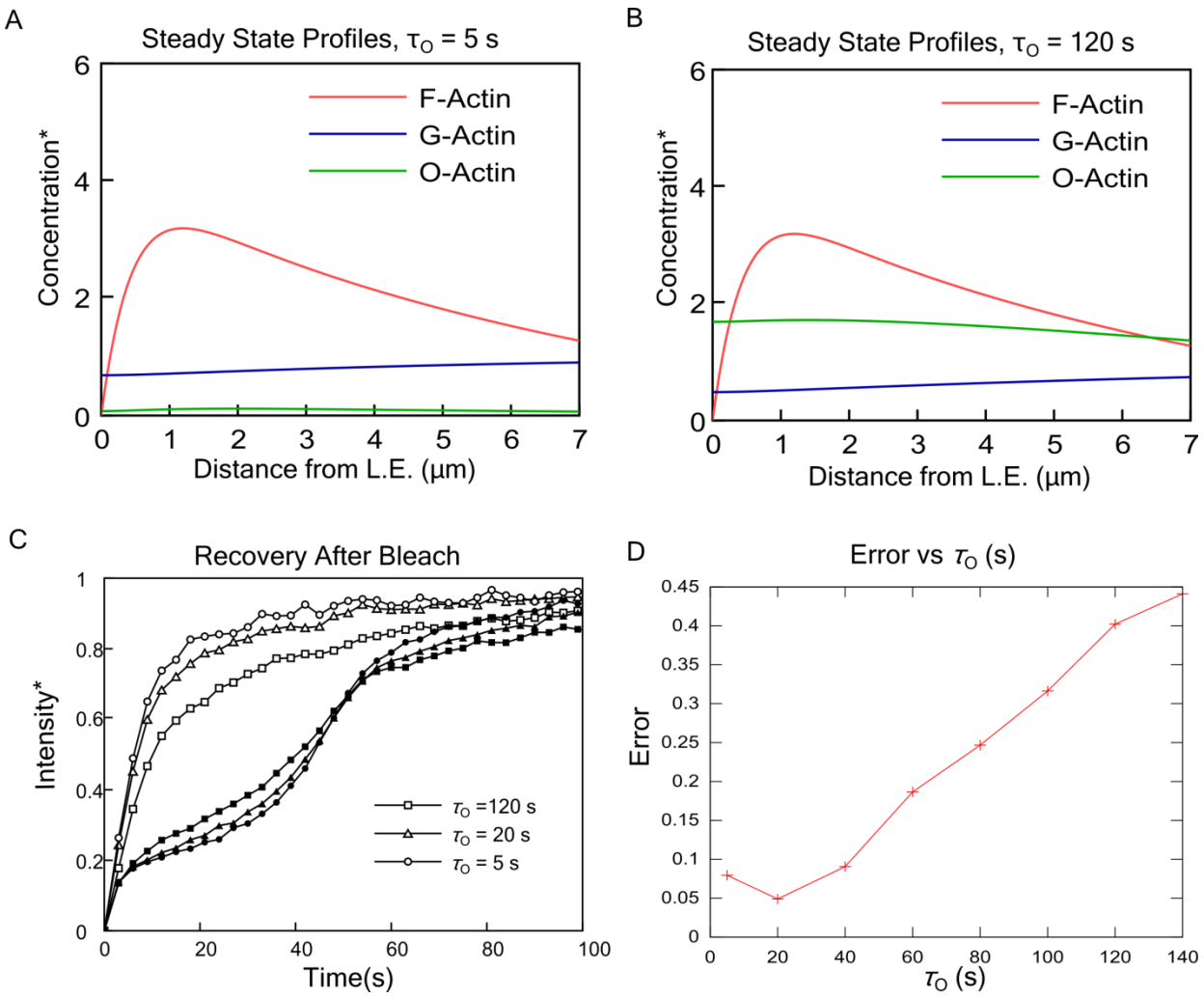


**Figure S8.** Effects on concentration profile and FRAP in model with oligomers due to changing oligomer lifetimes. All other parameters are kept the same as in Fig. 6. Profile plots for all three species with (A) $\tau_O$ = 5 s, and (B) $\tau_O$ = 120 s. (C) Recovery plot comparing three different recovery curves for the different $\tau_O$ (front: empty symbols; back: filled symbols). (D) Error for FRAP simulations compared to the experimental data of Fig. 2C.

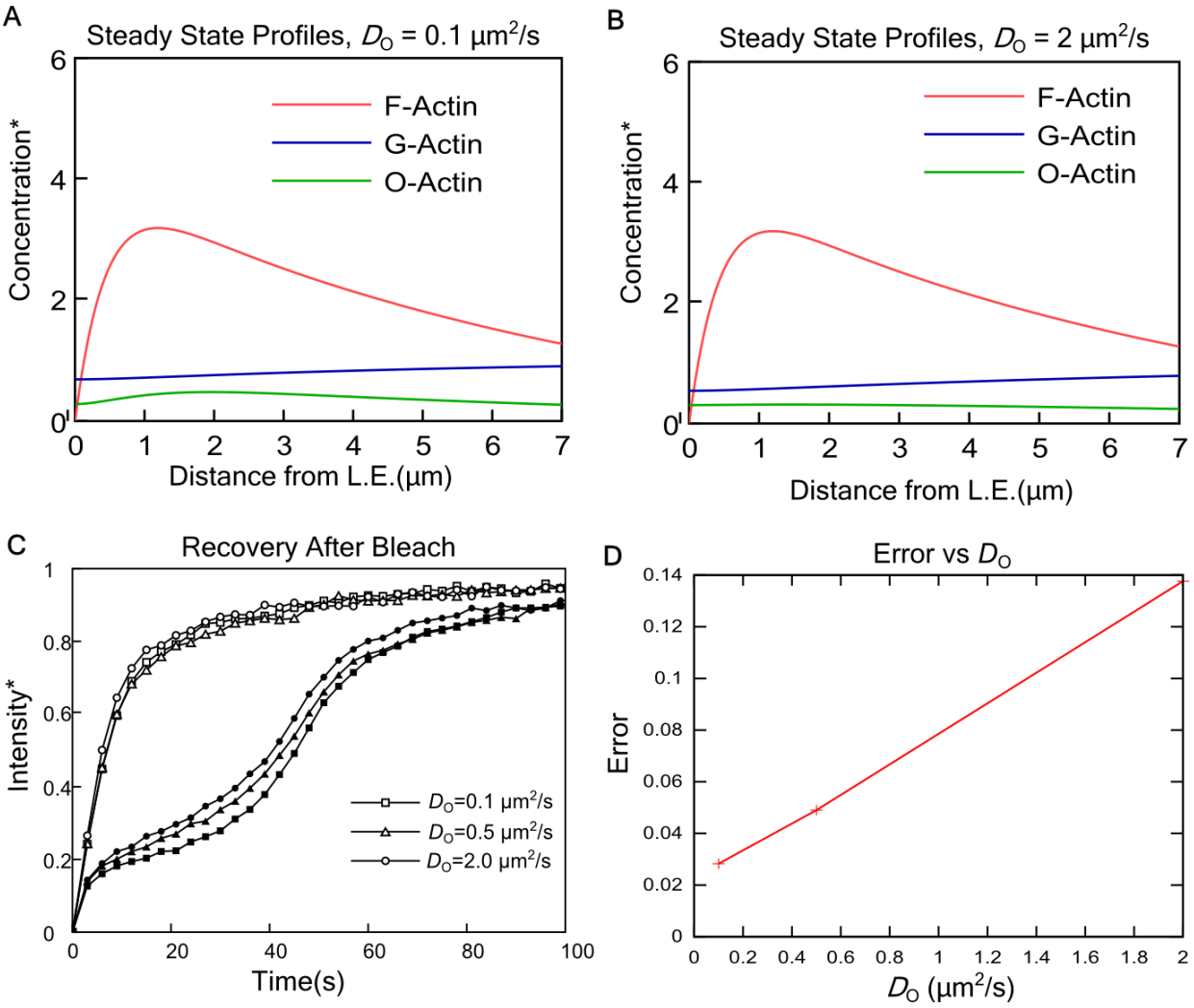


**Figure S9.** Effects on concentration profile and FRAP in model with oligomers due to changing oligomer diffusion coefficients. All other parameters are kept the same as in Fig. 6. Profile plots for species with (A) $D_O$ = 0.1 μm²/s and (B) $D_O$ = 2 μm²/s. (C) Recovery plot comparing three different recovery curves for the different $D_O$ (front: empty symbols; back: filled symbols). (D) Error for FRAP simulations compared to the experimental data of Fig. 2C.

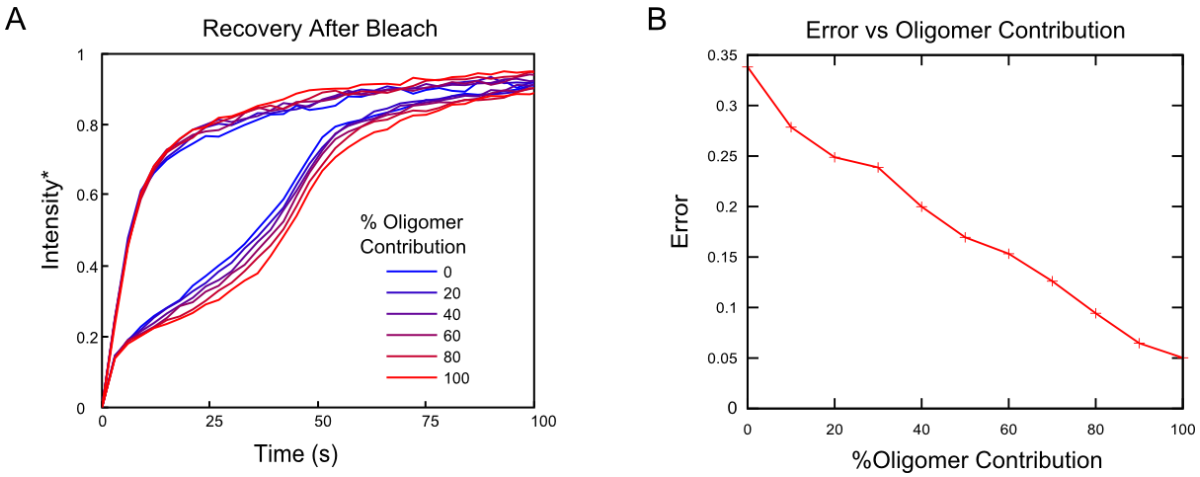


**Figure S10.** FRAP simulations varying the amount of oligomer contribution to the basal appearance rate. Recovery curves for different contributions of O-actin to the appearances away from the leading edge (fraction of $A_2$ term of Eq. 1 of main text). The recovery curves for low percentages of O-actin contribution are similar to the monomer-only model. The limit of 100% oligomer contribution is the case of Fig. 6. Zero contribution is similar to the monomer-only model (Fig. 4) but includes slowly-diffusing O-actin that does not associate. Parameters: $K$ = 0.5 $s^{-1}$, $v_r$ = 0.056 μm/s, $D_O$ = 0.5 $\mu m^2/s$, $D$ = 4 $\mu m^2/s$. Reducing the appearance rate of oligomers causes an accumulation of oligomers, which cannot polymerize; to balance this effect parameter $\tau_O$ was adjusted to keep the F-, G- and O-actin concentrations similar to those in Fig. 5C. The value of $\tau_O$ was 3.3, 5.7 and 20 s at 0%, 50% and 100% O-actin appearances, respectively. (B) Error for FRAP simulations compared to the experimental data of Fig. 2C.

## References


1. Zicha, D., I. M. Dobbie, M. R. Holt, J. Monypenny, D. Y. Soong, C. Gray and G. A. Dunn. 2003. Rapid actin transport during cell protrusion. Science 300:142-145.
2. Smith, M. B., H. Li, T. Shen, X. Huang, E. Yusuf, and D. Vavylonis. 2010. Segmentation and Tracking of Cytoskeletal Filaments using Open Active Contours. Cytoskeleton 67:693-705.
3. Ryan, G. L., H. M. Petroccia, N. Watanabe, and D. Vavylonis. 2012. Excitable actin dynamics in lamellipodial protrusion and retraction. Biophys J 102:1493-1502.
4. Watanabe, N., and T. J. Mitchison. 2002. Single-Molecule Speckle Analysis of Actin Filament Turnover in Lamellipodia. Science 295:1083-1086.
5. Kiuchi, T., T. Nagai, K. Ohashi, and K. Mizuno. 2011. Measurements of spatiotemporal changes in G-actin concentration reveal its effect on stimulus-induced actin assembly and lamellipodium extension. J Cell Biol 193:365-380.


## Movies

**Movie S1.** Example of FRAP experiment, showing the cell in Fig. 2. Left: mCherry-actin; right: EGFP-actin. The time interval between frames is 3 sec.The exposure time is 750 ms for EGFP-actin and mCherry-actin. A 435 nm laser was irradiated ten times within 300 ms after the 10th frame, and then the 11th frame was acquired immediately.The images were enlarged by intermediate lens (1.6X). The pixel size is 100 nm.

**Movie S2.** Simulated FRAP in model with monomers as only diffuse actin. Movie corresponds to Fig. 4C. Frames are separated by 3 sec. Simulated exposure time is 500 ms and 1 pixel = 100 nm. Bleached region is 5 x 20 μm.

**Movie S3.** Simulated FRAP in model with both monomers and oligomers as diffuse actin. Movie corresponds to Fig. 6C. Frames are separated by 3 sec. Simulated exposure time is 500 ms and 1 pixel = 100 nm. Bleached region is 5 x 20 μm.